buildings

MDPI

Article

Shape Memory Polymer Foam for Autonomous Climate-Adaptive Building Envelopes

Mario Walter [1], Kristin Lengsfeld [2,*], David Borschewski [3,4], Stefan Albrecht [3], Philipp Kölsch [2], Thorsten Pretsch [1], Martin Krus [2] and Susanne Lehmann-Brauns [5]

1 Department Shape-Memory Polymers, Fraunhofer Institute for Applied Polymer Research IAP, Geiselbergstrasse 69, 14476 Potsdam, Germany
2 Department Hygrothermics: Moisture and Thermal Control, Fraunhofer Institute for Building Physics IBP, Fraunhoferstrasse 10, 83626 Valley, Germany
3 Department Life Cycle Engineering, Fraunhofer Institute for Building Physics IBP, Nobelstraße 12, 70569 Stuttgart, Germany
4 Department Life Cycle Engineering, Institute for Acoustics and Building Physics, University of Stuttgart, Nobelstraße 12, 70569 Stuttgart, Germany
5 Department Innovation Management, Fraunhofer Institute for Building Physics IBP, Fraunhoferstrasse 10, 83626 Valley, Germany
* Correspondence: kristin.lengsfeld@ibp.fraunhofer.de

Abstract: Reducing the continuously growing cooling energy demand of buildings is an important part of achieving global emission targets. Here, we present an innovative scenario of how the integration of a programmable material into a climate-adaptive building envelope (CABE) can create an energy-efficient thermal management system inherent to the material. This novel concept is based on a thermoresponsive shape memory polymer foam (SMP) and is designed to regulate the flow of ambient air through the building envelope in order to enable natural cooling of the structure. Hygrothermal simulation data obtained by the software WUFI® Plus indicate that significant cooling energy saving potential may be accessible with this type of concept. As a possible material basis for a corresponding adaptive element, a reactive foamed polyurethane-based SMP foam is proposed, which is capable of executing a thermoreversible shape change of more than 20% while having a suitable switching temperature range. Finally, the ecological impact of such a functional foam element is evaluated in detail as well as its influence on the overall balance of a façade construction by means of a life cycle assessment (LCA).

Keywords: adaptive building envelope; programmable materials; inherent thermal management; shape memory polymer foam; hygrothermal simulation WUFI®; life cycle assessment

check for updates

Citation: Walter, M.; Lengsfeld, K.; Borschewski, D.; Albrecht, S.; Kölsch, P.; Pretsch, T.; Krus, M.; Lehmann-Brauns, S. Shape Memory Polymer Foam for Autonomous Climate-Adaptive Building Envelopes. *Buildings* **2022**, *12*, 2236. https://doi.org/10.3390/buildings12122236

Academic Editor: Xing Jin

Received: 15 November 2022
Accepted: 6 December 2022
Published: 15 December 2022

1. Introduction

The reduction in energy consumption and the associated CO_2 emissions is a key to achieving global climate targets and limiting global warming. Currently, one of the largest consumers is the construction sector, which accounts for 36% of total energy demand and 39% of energy- and process-related CO_2 emissions [1]. More than 15% of the consumption of the building sector is related to the operation of air conditioning systems [2], which are thus responsible for CO_2 emissions of more than 1000 Mt annually [3]. Not only because of global warming, a continuous growth is assumed for the upcoming years. For example, the International Energy Agency predicts an energy demand for building cooling of 6200 TWh in 2050, which will represent 16% of global consumption and would be equivalent to a doubling of CO_2 emissions [3]. The demand for indoor cooling is determined by the prevailing climatic conditions, whereas the amount of energy required for this purpose depends largely on the structural conditions. In addition to purpose-designed buildings, the insulation properties of the building envelope play a decisive role. Traditional insulation is a static construction that reduces the flow of heat through a wall and thus ensures that the rise in internal temperature is greatly limited during the very warm periods of the year. However, such insulation also prevents heat accumulated inside from being transferred to the outside. While this is desirable during heating periods when outdoor temperatures are low, it also results in higher energy consumption during cooling periods in order to achieve the desired indoor thermal comfort conditions. A promising solution is offered by climate-adaptive building envelopes (CABEs), which adaptively respond to the ambient conditions. Plenty of concepts have been developed in the last decade [4–7], and their effectiveness has been demonstrated using different simulation approaches [8–11].

Several of these systems utilize sensors and actuators for control, thus imposing an additional demand for energy and, crucially, electronic components [12–15]. Within the framework of SFB1244 "Adaptive Envelopes and Structures for the Built Environment of Tomorrow", research is being conducted on adaptive façade concepts, among other things, also using sensors and actuators [16]. In this context, the initial approaches by Refs. [17,18] were also analyzed in terms of their building physics characteristics, and their potential in terms of their environmental impact was considered by means of a life cycle assessment. Innovative solutions based on smart materials open up the possibility of implementing adaptivity into building envelopes. Some promising solutions include the use of hydrogels [19–21], thermo-bimetals [22,23], thermochromic coatings [10,24], phase change materials [25–27], shape memory alloys [28,29], as well as shape memory polymers (SMP) [30,31]. Due to their molecular structure and morphology, the latter are able to undergo a temperature-dependent reversible shape change, which is also known as so-called two-way shape memory effect (2W-SME) [32–38]. Such materials have been repeatedly discussed, e.g., in the context of adaptive shading systems capable of autonomously regulating the amount of irradiated sunlight [39,40].

While the benefits of adaptive shading systems have been widely demonstrated [10,41–44], they are accompanied by the disadvantage of preventing not only unwanted heat but also necessary light from entering the building, usually requiring additional energy for artificial lighting. Moreover, they do not solve the problem of heat accumulated inside the building during the hot phase of the year.

Recently, some of us presented a novel approach in which thermoresponsive actuation of a SMP foam can be utilized to control the opening and closing of ventilation channels as a function of temperature, thus enabling the switching of convection through the façade from "ON" to "OFF" and vice versa in the course of temperature cycling [45]. Such systems have the potential for use in façade constructions. When the outside temperature is too high, a flow through the façade structure may be initiated by opening apertures, which removes part of the excessive heat via a convective flow, thus reducing the cooling demand. This programmable thermal conductivity may hold the key to implementing material-inherent thermal management directly into the façade, providing significant potential for energy savings.

To further increase the attractiveness of our solution, and thus, its application relevance, a façade construction is virtually designed in which such an adaptive element can be integrated in a target-oriented way. Based on this, the energy demand for indoor climate control is simulated with the hygrothermal software tool WUFI® Plus [46,47] for different climatic conditions with and without the consideration of adaptivity of the building envelope in order to reveal the energy saving potentials. In the next step, a novel formulation for a SMP foam is developed, focusing on pronounced bidirectional actuation and suitable switching temperatures. In order to enable a holistic evaluation of such a CABE concept, the ecological impact of the SMP foam in comparison to conventional rigid polyurethane (PU) foams, as well as the influence on the overall environmental profile of the façade construction, including the use phase, are additionally calculated in the form of a life cycle assessment (LCA).

2. Materials and Methods

To evaluate the concept of a façade with material-inherent thermal management, a model is designed to simulate the influence of a switchable rear ventilation on the indoor climate for different climatic scenarios. The following section describes how the different aspects to be taken into account, namely energy saving potential, functionality and sustainability, are investigated and analyzed.

2.1. Hygrothermal Simulation

As the basis for the simulation, an envelope construction is chosen, which includes an air layer between an external thermal insulation composite system (ETICS) and the wall. Depending on the thermal conditions, an air exchange of this layer with the environment is either enabled or disabled. This functionality is to be implemented in the final application by integrating an SMP element into the façade construction.

When the switching condition is reached, the air exchange is "activated", and an airflow, mainly driven by thermal buoyancy, is initiated ventilating the air layer between the wall and the ETICS. In this way, a night-time cooling of the wall construction is possible—unnoticed by residents. Based on this scenario, a whole building simulation using WUFI® Plus is performed to check the principle's feasibility and benefits.

2.1.1. Building Environment and Façade Design

A residential unit in a multi-story apartment building with a total wall height of 10 m is chosen as the building environment. Considering the conditions common for Europe, traditional brick walls are implemented as the basic framework of the building. For the apartment, a two-room design is selected as a simplification, consisting of a large and a small room with 160 m^2 and 45 m^2 areas, respectively (Supplementary Materials: Figure S1). The calculations are conducted for the larger of the two rooms, which is equipped with four windows each facing north and south, and three windows on the east and west sides. Each window has an area of 1.2 m^2 and a total U-value (heat transfer coefficient) of 2.73 $W{\cdot}(m^2{\cdot}K)^{-1}$. The defined wall construction with the ventilated ETICS is shown in Figure 1, while the specifications are given in Table 1.

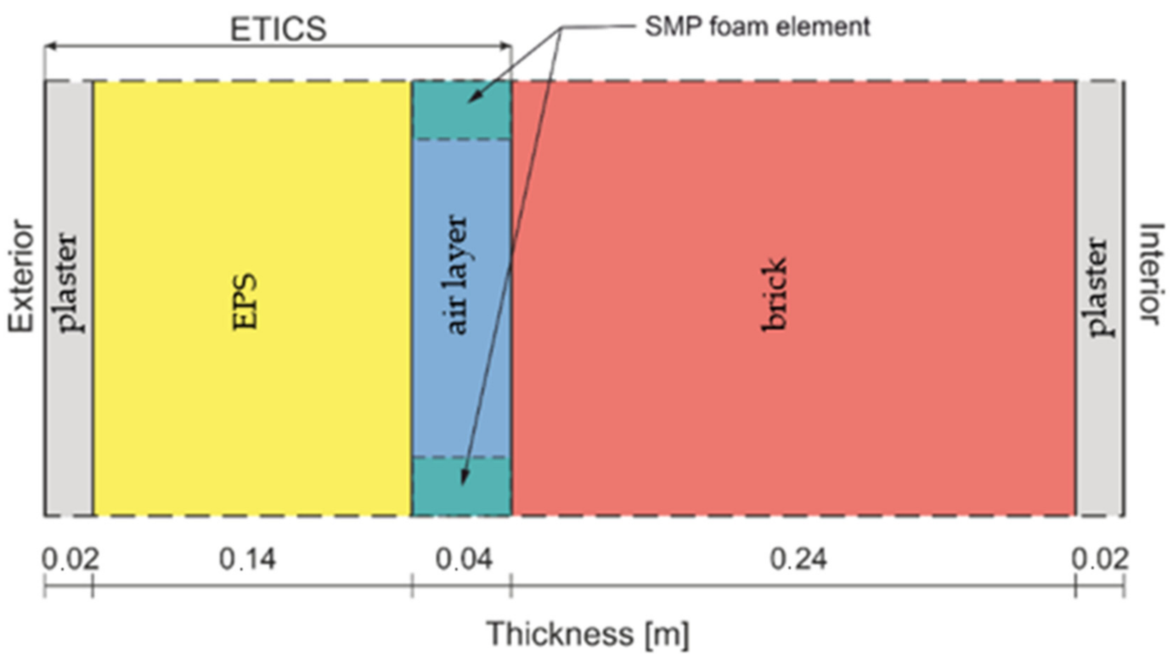

Figure 1. One-dimensional cross-section of the defined wall construction with the ETICS and the ventilation space behind, as well as the foam elements.

Table 1. Materials, layer thicknesses and thermal conductivities of the wall materials.

Thickness [m]	Material	Thermal Conductivity [W·(m·K)$^{-1}$]
0.02	Cement Rendering	1.2
0.14	Expanded Polystyrene (EPS)	0.04
0.04	Air Layer	0.23
0.24	Solid Brick Masonry	0.6
0.02	Gypsum Rendering	0.2

The floor and the ceiling are reinforced concrete elements with impact noise insulation and a screed layer on top. These elements are defined as adiabatic, which means that the same indoor climatic conditions prevail in the apartment above and below the respective room. The foam elements are positioned at the upper and lower ends of the air channel. Their thermoresponsive shape change enables temperature-dependent opening and closing of the same.

2.1.2. Investigated Locations

To evaluate the performance and the possible effects of the ventilated ETICS under different climatic conditions, three different locations are investigated. The coldest location, with an annual mean temperature of 6.6 °C, is Holzkirchen in Germany [48]. Due to its closeness to the Alps and an altitude of 690 m above sea level, it belongs to the moderately cold regions. The second German location is Freiburg im Breisgau. It is located on the Upper Rhine (altitude 278 m) and is one of the most sun-rich cities in Germany. With an annual mean temperature of 10.4 °C, the climate here is significantly warmer than in Holzkirchen [48]. Madrid in central Spain is selected as the third location. With an annual mean temperature of 14.3 °C (altitude 667 m), it has the warmest climate in comparison and is a representative example of warmer locations in southern Europe [48]. Figure 2 summarizes the annual outdoor air temperatures of the three selected locations.

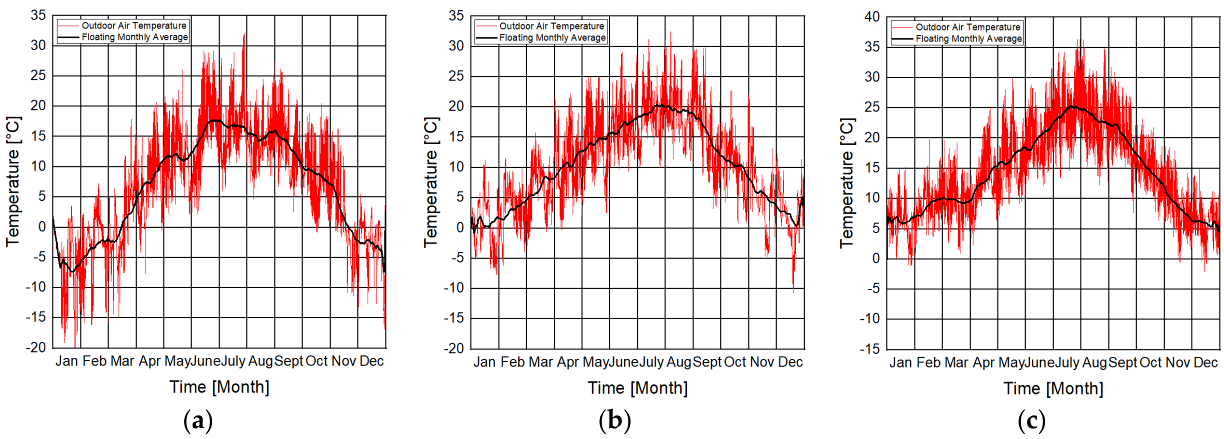

Figure 2. Outdoor air temperatures for (**a**) Holzkirchen (DE), (**b**) Freiburg (DE) and (**c**) Madrid (ES) as hourly mean values (red curve) and floating monthly average (black curve) [48].

2.1.3. Simulation Parameters

On the exterior of the walls, the climatic data of the three locations are applied. The ceiling and the floor of the apartment are adiabatic. The long-wave radiation cooling is not explicitly calculated for the wall surfaces but implicitly considered by the effective heat transfer coefficient, while short-wave radiation is considered in a measure to be expected for a render of medium brightness. In a normal urban environment, overcooling effects due to, e.g., long-wave radiation losses during night time, as can be observed on roof constructions, are of subordinate relevance. For the indoor climate, an ideal heating system is assumed, which heats up the apartment constantly to 20 °C, as soon as required. In a second simulation run, the cooling energy demand with an additional ideal space cooling to 22 °C was determined. The relevant parameters for the simulations are given in Table 2.

Table 2. Simulation parameters and coefficients.

Parameter	Values/Datasets
Outdoor climate	Holzkirchen (DE); Freiburg (DE); Madrid (ES)
Heat transfer coefficient external wall	$25\ W\cdot(m^2\cdot K)^{-1}$
Short-wave radiation absorptivity	0.4
Explicit radiation balance	Not used
Indoor climate	Simulation result
Heat transfer coefficient internal wall	$8\ W\cdot(m^2\cdot K)^{-1}$
ACH * inside the apartment	$1\ h^{-1}$
Target temperature heating	20 °C (ideal system)
Target temperature cooling	22 °C (ideal system)

* ACH—air change rate in air changes per hour.

To date, WUFI® Plus is not able to perform simulation in connection with temperature-dependent transient air change rates by itself. Therefore, first of all, the simulation of the apartment is performed under the respective climatic conditions for each location without a ventilation behind the ETICS. The results of these simulations are the hourly air temperatures in the ventilation gap. In reality, the SMP foam element will actuate in a switching range, reaching full opening at the upper temperature and a fully closed state at the lower temperature. In WUFI® Plus, however, it is to date not possible to simulate different temperature values as switching criteria for the activation and deactivation of the ventilation. Such an implementation requires a complex reprogramming of the software. For this reason, the corresponding temperature hysteresis has to be omitted at this point (for now). Consequently, the calculated cooling effect will be lower than in reality with hysteresis. Nevertheless, the calculations are appropriate to show to what extent the selected approach of achieving a temperature-dependent ventilation by means of a 2W-SMP foam may provide advantages with regard to summer heat protection. The switching criterion was defined as follows.

In a case where the outside temperature drops below 20 °C, and the inside temperature at the same time shows a value above 20 °C, the criterion is fulfilled. As a result, air exchange with the environment is enabled (Figure 3). In this way, in the event of excess temperature inside the building, cooler periods of the day can be used to dissipate excessive heat. By using a natural cooling process, the cooling energy could consequently be saved.

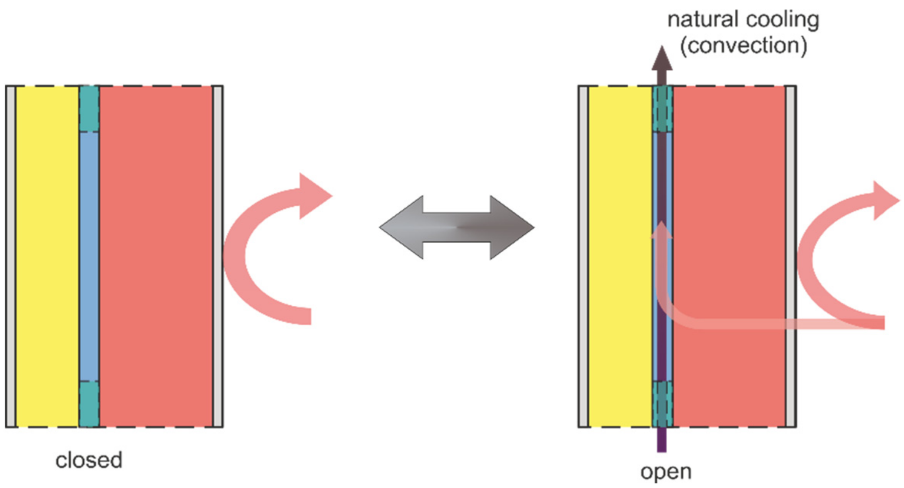

Figure 3. Schematic illustration of an adaptive ventilated ETICS with the closed foam elements (**left**) and the opened ones enabling convection through the façade (**right**).

The difference between the temperature in the air layer inside the ETICS and the ambient temperature results in a difference in air density, which acts as a driving force for thermal buoyancy. With the help of the differential pressure, the wall height and the width of the air layer gap, the theoretical airflow velocity can be calculated. However, the pressure drop in the air layer gap increases with the square of the airflow velocity. Therefore, an iteration process is needed to determine the resulting airflow velocity, and herewith, a transient hourly air change rate (ACH). During the iteration process, the convergence criterion is met when the pressure drop in the air layer gap is as high as the pressure difference caused by the thermal buoyancy. The resulting ACH are always calculated for the western façade with the highest temperatures caused by the coincidences of strong radiation loads from the setting sun and high outdoor air temperatures in the afternoon. For simplification, it is assumed that the driving force pressure is completely used up on the way to the air layer gap. For the intended considerations, the developed procedure is assumed to be sufficiently accurate.

2.2. Shape Memory Polymer Foam and Adaptive Element

In order to implement the described adaptivity of the building envelope to the environmental conditions, a PU-based SMP foam is developed, which is able to execute thermoreversible shape changes. A suitable switching temperature range, through which the switching condition of the simulation model can be addressed, represents the most important criterion here, in addition to pronounced actuation. This provides the basis for subsequent transferability into the application.

2.2.1. Foam Preparation

In view of its thermal properties, the commercially available polyol Diexter G240 from C.O.I.M. (Offanengo, Italy) is selected as the soft segment (SS) building block. It is a linear polyol, which consists of poly(1,6-hexylene adipate) (PHA) with a molecular weight of 2970 $g{\cdot}mol^{-1}$. The polyester diol shows a melting and crystallization peak temperature of 57.8 °C and 40.4 °C, respectively, and has an enthalpy of fusion of 105.0 $J{\cdot}g^{-1}$. The hard segment (HS) is composed of the isocyanate 4,4′-diphenylmethane diisocyanate (MDI) and the crosslinker diethanolamine (DEA). The foaming reaction is carried out according to the prepolymer method as a one-pot two-step reaction. Deionized water is used as the blowing agent. A slight excess of MDI with a ratio of NCO/OH = 1.03 is employed. Due to the relatively low reactivity of the polyester diol toward MDI compared to the blowing agent of deionized water and the DEA, the very active catalyst dibutyltin dilaurate (DBTL) is utilized to ensure a complete coupling between HS and SS.

Detailed information on the utilized materials and the synthesis procedure can be found in Appendix A.1.

2.2.2. Characterization Methods

Various methods are used to characterize the physical properties of the foam. The density is determined with the aid of an analytical balance (AEJ 100, Kern & Sohn GmbH, Balingen-Frommern, Germany). A total of five measurements are performed on cube-shaped samples, which have a dimension of $10 \times 10 \times 10$ mm^3, and the results are averaged. Basically, sample density is calculated from the ratio between the weight and volume of each sample.

The closed cell ratio is estimated using a rapid test method developed in-house. This involves measuring the buoyancy of cuboidal samples in a silicon oil after a soaking time of 72 h. A special low-viscosity silicon oil (Ebesil Öl B 0,65, Quax Gmbh, Otzberg, Germany) is used. This ensures that complete flooding of the open cells is guaranteed.

For the determination of thermal conductivity according to a standard, a self-designed hot plate apparatus is used [49]. The required sample size with a cross-sectional area of 150×150 mm^2 and a height of 20 mm is achieved by combining several smaller sized samples.

In order to investigate the phase transitions of the SS of the foam as well as its isothermal crystallization behavior, differential scanning calorimetry (DSC) is performed using a Q100 DSC device (TA Instruments, New Castle, DE, USA).

The thermomechanical properties and actuation behavior of the foam are investigated using dynamic mechanical analysis (DMA). Experiments are performed on cube-shaped samples with an edge length of about 10 mm using a Q800 DMA from TA Instruments (New Castle, DE, USA). Thermomechanical tests are conducted to evaluate the mechanical properties, hardness and compressive strength of the foam at 20 °C and 45 °C, respectively.

To determine the shape memory properties and their factors of influence, the samples are initially programmed and then thermally cycled under constant load conditions between an upper and a lower temperature. The experimental parameters are varied in a targeted manner to evaluate the extent of actuation. Therefore, the upper temperature T_{high} is varied between 35 °C and 55 °C, the lower temperature T_{low} between 0 °C and 20 °C, and the external load F between 0.5 N and 10 N. The load is applied in such a way that the foam is compressed along its rising direction. In addition, the durability of the functionality is verified in a multi-cycle experiment with 30 consecutive cycles in an application-related temperature scenario between 15 and 40 °C.

The thermoreversible strain ε_{rev} is the key parameter in the study of actuation in polymers. For foams, it is defined for each individual temperature cycle according to Equation (1) as the absolute change in height of a sample.

$$\varepsilon_{\mathrm{rev}}(\mathrm{N}) = \frac{h_{high}(\mathrm{N}) - h_{low}(\mathrm{N})}{h_{low}(\mathrm{N})} \times 100\% \tag{1}$$

A detailed description of the procedures applied is available in Appendix A.2.

2.2.3. Adaptive Element

To transfer the characterization results into an application demonstrator, foam specimens with the dimension of $10 \times 50 \times 45$ mm^3 and an internal aperture of ellipsoidal shape (height 6.0 mm, width 20.0 mm) are produced with an Epilog Zing laser cutter (Epilog Laser, Golden, CO, USA). The design is created using CorelDRAW 2019 (Corel Corp., Ottawa, Canada) software. Experimental investigations on adaptive elements with foam samples are carried out in a temperature chamber TH2700 (Thümler GmbH, Nürnberg, Germany). A self-designed sample holder is used for this purpose. In the first step, a sample is heated to T_d = 55 °C, and a metal cylinder is placed on the foam, which applies a constant load of 200 g. The ratio of mass to foam area is 40 g·cm^{-2}. This value corresponds to a stress of 3.9 kPa. Then, the actuation of the foam at varying temperatures between T_{high} = 55 °C and T_{low} = 10 °C is investigated.

2.3. *Life Cycle Assessment*

With the purpose of the ecological evaluation of the SMP foam as well as the CABE concept, the different contributing factors in the production and use phase are computed, and, based on this, an evaluation is elaborated.

The most relevant method to systematically analyze environmentally relevant impacts is the life cycle assessment (LCA). It is standardized in the ISO 14040 [50] and ISO 14044 [51] standards. The basis for the analysis is the capture of all relevant material flows that can be assigned to a product or service for its entire life cycle, e.g., energy consumption and raw material use or direct emissions into the environment. The impacts caused by these input and output flows are then quantified using standardized impact indicators (e.g., CO_2 footprint). The latest software version of GaBi software is used as standard to create and evaluate life cycle assessments [52].

Fraunhofer IBP's own software tool GENERIS® [53] for life cycle building assessment is available for balancing the building and building operation (heating, cooling, ventilation). GENERIS® enables the preparation of life cycle assessments in accordance with the current standardization and in compliance with the DGNB [54] and BREEAM [55] certification systems for sustainable buildings. It can also provide decision support during the design process. It is based on datasets from the ÖKOBAUDAT, a database [56] the Federal Ministry of the Interior and Community (BMI) provides. The datasets comply with DIN EN 15804 [57] and are aimed at all stakeholders interacting with the LCA of buildings.

The efforts for production, construction and disposal are examined in accordance with DIN EN 15978:2012-10 [58]. The construction is modeled in the GENERIS® software and is based on ÖKOBAUDAT datasets (Release 2021-I).

To assess the use phase, the energy demands for heating and cooling, calculated in the thermal simulation, are covered by an electric heat pump. The seasonal coefficient of performance (SCOP) is assumed to be 4.9 with an assumed seasonal energy efficiency ratio (SEER) of 4.7. A dynamic environmental profile for electricity is used in the assessment. For better comparability, the same profile is used for all three locations.

With the end of life, mineral construction materials are processed in a building rubble processing plant. The insulation material and SMP are incinerated for the generation of thermal energy and electricity.

3. Results

3.1. Hygrothermal Simulations

In the following section, the calculated results for the three selected locations—Holzkirchen (DE) with the coldest climatic conditions, Freiburg (DE) as an example of the warmest conditions in Germany and Madrid (ES) as representative of a hotter climate in the southern European mainland—are presented in a comparative analysis.

The first point to evaluate are the resulting ventilation rates behind the ETICS. The time when the switching criterion is fulfilled in combination with the strength of the ACH rate gives a first hint toward the functionality and suitability in each investigated climate. The annual numbers of hours when ventilation occurs, the corresponding annual percentage, as well as the mean annual ACH rate are given in Table 3.

Table 3. Hours of ventilation and mean annual ACH on the west-oriented façade.

Location	Annual Ventilating Hours [H]	Annual Percentage [%]	Mean Annual ACH [h^{-1}]
Holzkirchen	1022	11.66	9.67
Freiburg	1709	19.51	21.05
Madrid	1848	21.10	49.27

It is obvious that Holzkirchen has the lowest number of annual ventilating hours, the lowest mean annual ACH rate and, with a max. of 500 h^{-1}, the lowest peaks of the hourly ventilation rates (Supplementary Materials: Figure S2). This is not surprising, as Holzkirchen is the coldest of the investigated outdoor climates. Much more interesting is the comparison between the locations of Freiburg and Madrid. Both locations are in completely different climatic zones and have, with an annual difference of approx. 1.6%, nearly the same amount of annual ventilation hours. It seems that due to the higher temperature differences between the ventilation space and the outdoor temperature, the ventilation rate is mainly influenced. Here, Madrid shows peak values in the hourly ventilation rate nearly twice as large as Freiburg (Supplementary Materials: Figures S3 and S4). The mean annual ACH rate in Madrid is also almost a factor of 2.5 higher than in Freiburg.

The next aspect to be analyzed is the temperature in the air layer gap behind the ETICS. As to be expected from the climate data, the values for Madrid exceed those for Freiburg, while Holzkirchen shows the lowest values. This order is also reflected in the data for the annual average values presented in Table 4. Consequently, the mean annual temperature difference between the unventilated and the ventilated ETICS increases with the outdoor temperature. In other words, the higher the mean annual outdoor air temperature, the higher the temperature difference and the higher the annual number of hours with temperature difference. This ultimately leads to the conclusion that the benefits of the novel CABE concept generate a stronger impact in warmer climates. A detailed comparison of the annual temperature profile for the unventilated and ventilated cases for the climatic conditions considered is provided in the supplementary materials (Supplementary Materials: Figures S5–S7).

Table 4. Mean annual air temperatures in the air layer gap on the west-oriented façade.

Location	$T_{air,mean}$ * unventilated [°C]	$T_{air,mean}$ * ventilated [°C]	$\Delta T_{air,mean}$ * [K]	$t_{\Delta T}$ ** [K·h]
Holzkirchen	18.3	17.97	0.33	2931
Freiburg	19.21	18.54	0.67	5812
Madrid	20.98	19.62	1.36	11902

* $T_{air,mean}$—mean annual air temperature; ** $t_{\Delta T}$—annual number of hours with a temperature difference between unventilated and ventilated scenario.

The indoor thermal comfort represents a key factor for the evaluation of innovative building envelope concepts. To assess the influence of adaptivity, the operative room temperatures are simulated for the ventilated and unventilated scenario, without taking into account any additional air conditioning. After all, the ultimate goal is to make this redundant by means of an adaptive building envelope.

Since the influence of the ventilation of the façade is mainly limited to the hot season, it is reasonable to use an additional parameter for the evaluation in addition to the annual mean operative room temperature. Normally, the value for the hours of over-temperature, above 26 °C, provides quite a helpful indicator. However, this parameter is not applicable in our case, since such high temperatures are not observed in the German locations even in the unventilated scenario. Another commonly used value is the "degree–hours". It is calculated as the product of the annual mean operative room temperature and the number of hours in a year. Table 5 summarizes the results for the two selected parameters as well as the differences resulting from the implementation of adaptivity for all three locations. For a more detailed insight into the distribution of the differences over the course of the year, the graphs of the operative room temperature with and without ventilation of the ETICS over time are illustrated in Figures 4–6. Again, it is evident that the interior climate can be positively influenced by integrating a temperature-dependent switching capability with the façade. The extent to which this occurs, however, depends on the external climatic conditions and grows with increasing annual mean outdoor air temperature. While the degree–hours difference for Holzkirchen amounts to 1082 K·h, it goes up to 2874 K·h for Freiburg and reaches its highest value for Madrid with 6739 K·h.

Table 5. Annual mean operative room temperature and degree–hours for the three locations.

	Ventilated ETICS	Unventilated ETICS	Difference	Difference [%]
Holzkirchen				
$T_{oper,mean}$ * [°C]	20.11	20.23	0.12	−0.59
Degree–hours [K·h]	176,187	177,269	1082	−0.61
Freiburg				
$T_{oper,mean}$ * [°C]	20.33	20.65	0.32	−1.55
Degree–hours [K·h]	178,093	180,967	2874	−1.59
Madrid				
$T_{oper,mean}$ * [°C]	21.17	21.94	0.77	−3.51
Degree–hours [K·h]	185,524	192,263	6739	−3.51

* $T_{oper,mean}$—mean annual operative temperature.

For all locations, a switchable rear ventilation generates a shift of the operative room temperature toward lower values in the summer months and, at the same time, significantly reduces the peak temperatures. For the German locations, this results in a reduction in maximum temperatures of up to 2 K. For Madrid, an even greater reduction of more than 3 K can be observed. It can therefore be stated that for the scenario of an apartment without air conditioning, the operative room temperature can be reduced with the help of the presented CABE concept, and thus, the indoor comfort can be improved during the summer time.

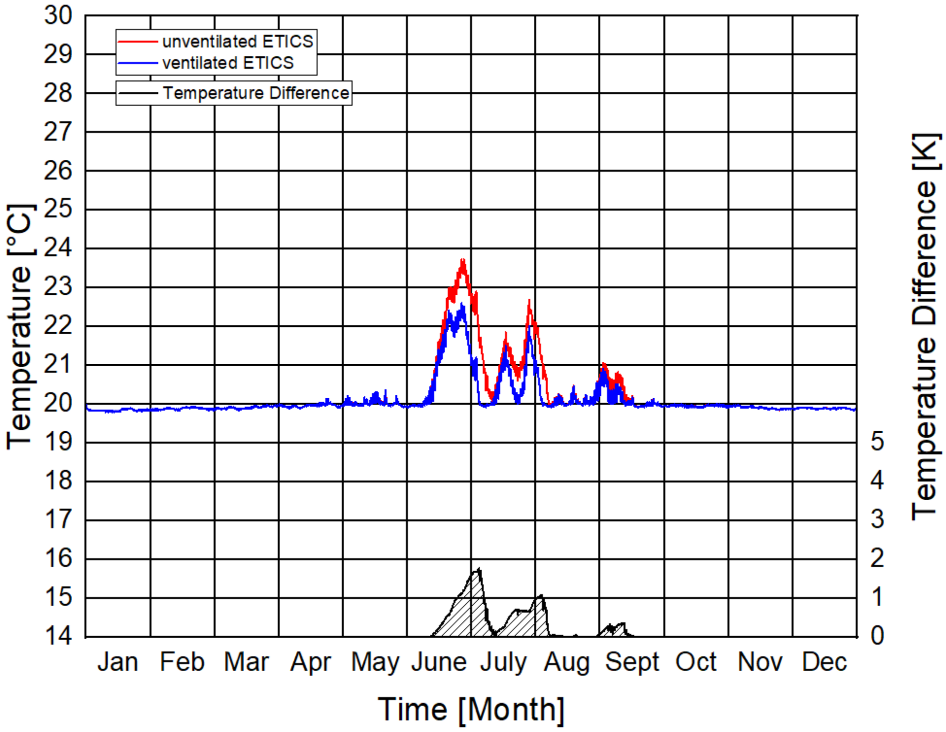

Figure 4. Operative room temperature with and without a ventilated ETICS for Holzkirchen (DE).

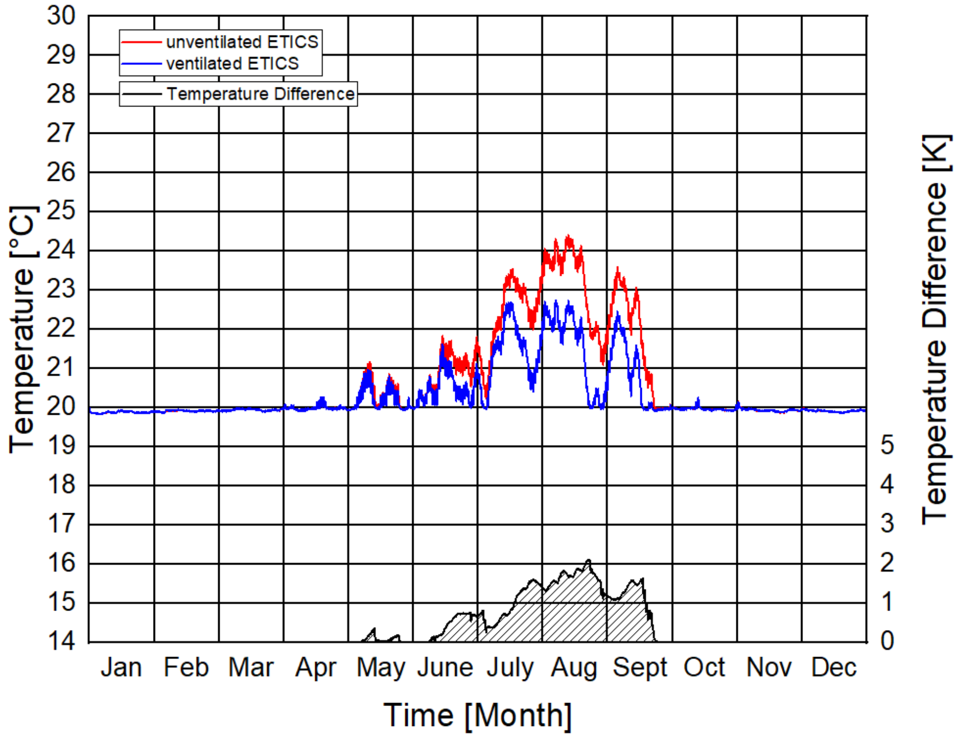

Figure 5. Operative room temperature with and without a ventilated ETICS for Freiburg (DE).

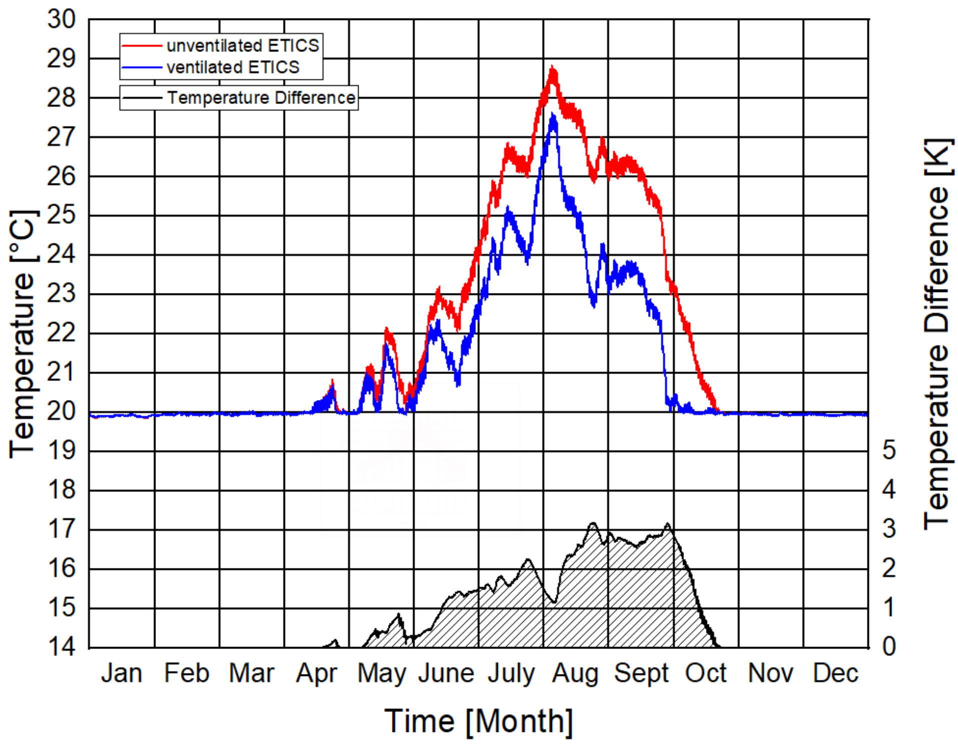

Figure 6. Operative room temperature with and without a ventilated ETICS for Madrid (ES).

The most interesting question to be answered is whether such a CABE concept can contribute to energy savings to a relevant extent. In order to answer this question, a further set of simulations are performed considering an ideal indoor air conditioning system. The ideal system always provides exactly the amount of cooling energy necessary to keep the interior at the desired target temperature of 22 °C without delay and restrictions. During the heating season, an ideal heating system provides the power to heat the apartment up to 20 °C in the same way.

Table 6 provides the results computed for the annual heating and cooling energy demand for the ventilated and unventilated ETICS, as well as the calculated deviations. As expected from the previous results, the adaptivity of the building envelope causes a significant decrease in cooling energy demand. An unexpected result is the observed trend that the percentage savings increase with colder climatic conditions. However, when considering the total saving amounts in kWh, they are clearly lower for the German locations than for Madrid. As a matter of fact, air conditioning is not part of the standard equipment in German residential buildings. Nevertheless, energy savings can theoretically indeed be attained by integrating a ventilated ETICS into the building envelope. In Madrid, where air conditioning is common, the exemplary saving amount for the investigated apartment with ventilated ETICS totals 662 kWh, which is a reduction of approximately 29% per year. This is a considerable contribution, especially considering the fact that it would be a natural and passive ventilation system without any auxiliary energy demand.

Another rather unexpected aspect is the slightly increased values for the heating energy consumption. Presumably, they can be explained by the selected boundary conditions of the simulation. On the one hand, the ventilation of the façade construction influences the subsequent simulation steps, and on the other hand, an ideal heating system is assumed, which constantly maintains the desired indoor temperature of 20 °C at all times. In case of a weather change to cooler outside temperatures during a warm phase when the ventilation is switched “ON”, situations may arise where the ACH cools down the wall. In this case, the heat stored in the brick wall is partially dissipated by convection in the air layer gap and, unlike in the comparative case, is not available. The result is a turn-on of the ideal heating system, and thus, an additional power consumption. However, since this case occurs mainly during short cooler periods in the summer phase, this is to be regarded as a virtual shortfall rather than a real problem. In the real-time application, the heating system is normally switched off, since a slightly lower indoor temperature is temporarily accepted. Therefore, it can be assumed that the additional energy demand can be neglected, and the evaluation should be based on the cooling energy demand.

Table 6. Annual heating and cooling energy demands and differences for the three locations.

	Ventilated ETICS	Unventilated ETICS	Difference	Difference [%]
Holzkirchen				
Heating Energy Demand [kWh]	12,300	12,146	+154	+1.25
Cooling Energy Demand [kWh]	185	336	−151	−44.94
Freiburg				
Heating Energy Demand [kWh]	9077	8912	+165	+1.82
Cooling Energy Demand [kWh]	482	807	−325	−40.27
Madrid				
Heating Energy Demand [kWh]	5293	5158	+135	+2.55
Cooling Energy Demand [kWh]	1652	2314	−662	−28.61

3.2. Shape Memory Foam and Adaptive Element

From the reaction of PHA diol with MDI, DEA, deionized water and the indicated additives, a foam with a density of 72 $g \cdot L^{-1}$, a porosity of 94% and a closed cell ratio of 64% is obtained. As can be seen in the associated light microscopic image, some of the pores have an elongated shape in the foaming direction and, for the most part, a width perpendicular to it in the range of 50 to 150 µm (Figure 7). As a result of the manual manufacturing process, several large pores can be observed.

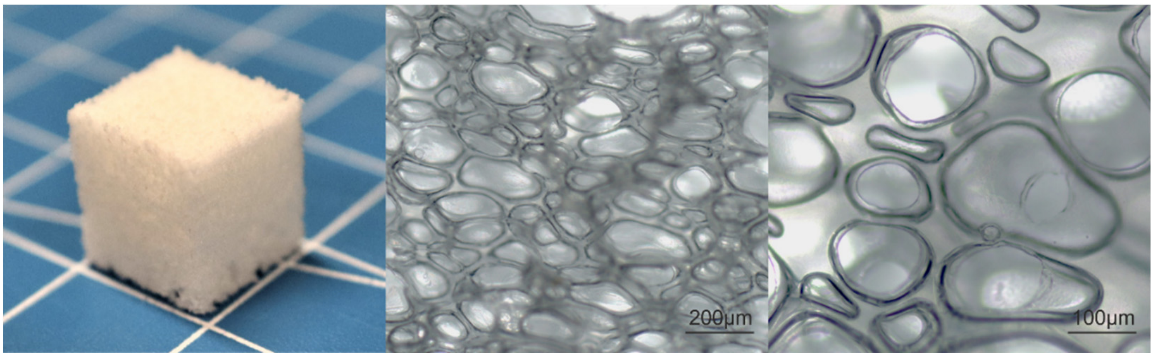

Figure 7. Foam cube sample of 10 × 10 × 10 mm^3 (**left**) and light microscope image of the pore structure with five-fold (**center**) and ten-fold zoom (**right**) with the foaming direction in horizontal orientation.

At the molecular level, the synthesis results in the formation of a phase-segregated block copolymer structure with so-called hard domains, arising from the reaction of MDI, DEA and deionized water, dispersed in so-called soft segments made from the polyester diol PHA. The hard segments are known to form physical net points due to the strong interactions in hydrogen bonds between the urethane and urea units. In addition, the crosslinking induced by DEA causes chemical net points to be formed simultaneously. As already observed in various other contexts, the formation of network structures leads to a reduced mobility of the chains, which in turn inhibits the crystallization of the soft segment [38,45,59,60]. Nominally, for the polyester-based soft segment, a peak crystallization temperature $T_{c,peak}$ of 5.4 °C was measured, corresponding to a drop in value of 35 °C compared to the pure PHA diol, while at the same time, a peak melting temperature $T_{m,peak}$ of 37.7 °C was determined, which was almost 20 °C below that of the pure polyester diol

(Table 7, Supplementary Materials: Figure S8). In addition, the melting enthalpy ΔH_m also experiences a significant reduction, dropping from 105.0 J·g^{-1} to 29.0 J·g^{-1} (Table 7). Despite the described limitations in chain mobility, the polyester phase is still able to crystallize at temperatures considerably higher than the $T_{c,Peak}$ determined by DSC. When selecting an isothermal crystallization scenario at 15 °C, the enthalpy of fusion decreases only slightly in the subsequent heating cycle. Even in the case of crystallization at an isothermal storage temperature T_{store} of 20 °C, it still reaches 84.9% of its original value (Table 7).

Table 7. Phase transition temperatures of the pure PHA and the PHA phase in PU foam, as detected by differential scanning calorimetry.

Material	T_{min} * or T_{store} [°C]	$T_{m,Peak}$ [°C]	$T_{c,Peak}$ [°C]	ΔH_m [J·g^{-1}]	$\Delta H_{m,iso}$ **/ΔH_m [%]	$t_{c,Peak,iso}$ *** [min]
PHA	−20	57.8	40.4	105.0	-	-
PU foam	−70	37.7	5.4	29.9	100	-
PU foam (isothermal)	5	37.9	-	29.1	97.3	2.1
	10	37.7	-	29.1	97.3	2.5
	15	38.3	-	28.8	96.3	3.2
	20	38.5	-	25.4	84.9	7.7

* T_{min}—end temperature of cooling cycle; ** $\Delta H_{m,iso}$—melting enthalpy after isothermal crystallization; *** $t_{c,Peak,iso}$—location of the crystallization peak during the 30 min crystallization phase.

In addition to the phase transition temperatures in the range of the temperature threshold of 20 °C selected as the switching criterion for the ventilated ETICS, the very good thermal conductivity λ of 0.040 W·(m·K)$^{-1}$ strengthens the qualification of the SMP foam for the addressed application. For comparison, the λ values of conventional insulation materials typically lie in the range of 0.020 to 0.050 W·(m·K)$^{-1}$ [61].

To determine the compression hardness, the foam was subjected to three consecutive cycles consisting of compression by 60% and subsequent unloading. The first two cycles were performed at 23 °C, and before the third cycle, the foam was heated to 45 °C to melt the soft segments. The room temperature measurements show the semi-rigid character of the foam, with 31.2 kPa and 57.2 kPa detected in the first cycle for compression hardness at 10% ($\sigma_{10\%}$) and 40% ($\sigma_{40\%}$), respectively. After unloading at the end of the first cycle, a compression set of 8.1% remains, which is due to cold programming of the polymer [62]. In addition, the $\sigma_{10\%}$ and $\sigma_{40\%}$ values decrease to 14.7 kPa and 49.6 kPa, respectively. This can be explained by the should-bend sites already present in the cell walls and struts at that time. Heating to 45 °C and the accompanying melting of the crystalline soft segments lead to a softening of the material and a drop in the $\sigma_{10\%}$ and $\sigma_{40\%}$ compression hardness to 6.2 kPa and 8.2 kPa, respectively. Above the melting temperature of the soft segment, the material hence behaves like a flexible foam.

In the next step, the functionality of the foam was evaluated. The variation of the upper and lower actuation temperature as well as the applied load, as the key experimental parameters, shows that the material exhibits a pronounced temperature-dependent actuation over a wide stress and temperature range and achieves values that have not yet been observed to this extent for foams (Table 8; Supplementary Materials: Figures S9 and S10). With an average value over three cycles for ε_{rev} of 22.7%, the highest value is observed at a stress of 5.4 kPa in a temperature range of 0 °C to 50 °C (Entry 5, Table 8, right).

Admittedly, it is also apparent that an intense mechanical loading results in a consistently higher rate of deformation in the second part of the force screening. As a result of the strong compression, a sort of mechanical conditioning of the matrix structure occurs on the one hand, and on the other hand, the contact between the cell walls, which are pressed against each other, intensifies. The attractive interactions that occur act as a counterforce to the restoring force of the polymer. This is also reflected in the growing compression set $\varepsilon_{residual}$ observed after a load-free recovery phase at elevated temperature. Nevertheless, the values are continuously above 17.5% during the repeated stress screen and again show their maximum of ε_{rev} = 19.6% at the same stress of 8.7 kPa as in the first stress screen. In order to mimic the influence of a continuous thermal load, the holding time at T_{high} was extended from 30 min to 10 h between two cycles. For the said reasons, this leads to a reduction in the actuation ε_{rev} from 17.6% to 16.2% (compare Entry 9 and 10, Table 8, left). This effect becomes even more evident when the compression stress is further increased, so that compression rates of above 80% are achieved (compare Entry 11 and 12, Table 3, left). Such an intensive compression leads to a distinct densification accompanied by increased sticking between the cell walls and struts, as a result of which, the compression set $\varepsilon_{residual}$ reaches values of up to 75%. Nevertheless, an actuation of 15.6% and 14.0%, respectively, can still be observed.

Table 8. Summary of measured values for reversible actuation ε_{rev} during a force screening with T_{high} = 60 °C and T_{low} = 0 °C (left) and temperature screening experiments under a stress of 5.4 kPa (right) showing the single values of the cycles for N = 1 to 3 and the average (avg) for each parameter set.

#	σ [kPa]	$\varepsilon_{rev,rel}$ [%]				$\varepsilon_{residual}$ [1] [%]	#	T_{low} [°C]	T_{high} [°C]	$\varepsilon_{rev,rel}$ [%]			$\varepsilon_{residual}$ [1] [%]
		N = 1	N = 2	N = 3	avg					N = 1	N = 2	avg	
1	4..4	9..9	11..6	12..5	11..3	1..1	1	0	55	22	22..9	22..4	<1
2	8..7	21..0	22..6	22..9	22..2	3..5	2	10 [4]	55	21..6	22..3	21..9	<1
3	13..1	19..3	20..0	22..9	20..7	21..5	3	15 [5]	55	20..2	20..7	20..5	<1
4	17..4	16..4	18..1	18..4	17..6	32..6	4	20 [6]	55	14	14..2	14..1	<1
5	4..4	17..7	17..9	17..8	17..8	33..1	5	0	50	22..1	23..3	22..7	<1
6	8..7	19..6	19..7	19..5	19..6	33..9	6	0	45 [4]	21	22..1	21..5	<1
7	13..1	18..5	18..3	18..5	18..4	35..3	7	0	40 [5]	17..6	19..5	18..6	<1
8	17..4	18..0	18..1	18..1	18..1	38..9	8	0	35 [6]	7..2	11..2	9..2	<1
9 [2]	4..4	17..6	-	-	17..6	-	9	15 [5]	40 [5]	16..2	18..7	17..5	<1
10 [3]	4..4	16..2	-	-	16..2	54..1	10	15 [7]	37 [7]	10..5	14..1	12..3	14..9
11	43..5	15..5	15..7	15..6	15..6	68..2	11	20 [7]	40 [7]	15..1	15..8	15..5	<1
12	87..1	13..8	14..1	14..1	14	75..5							
13	4..4	8..2	7..6	7..3	7..7	75..8							

[1] compression set after recovery for 15 min at σ = 0 kPa and T = 60 °C; [2] single cycle for verification of load influence; [3] single cycle after 10 h holding time under load at 60 °C; [4] equilibration time of 45 min; [5] equilibration time of 60 min; [6] equilibration time of 75 min; [7] equilibration time of 120 min.

Furthermore, the experiments on the variation of the actuation temperatures demonstrate that the temperature window can be significantly reduced without a substantial decrease in actuation. Raising T_{low} from 0 °C to 15 °C as well as decreasing T_{high} from 55 °C to 45 °C leads to a decrease in ε_{rev} by less than 10% (Entry 3 and 6, Table 8, right). In the temperature window between 15 °C and 40 °C, which represents the expected values in a façade quite well, a strong actuation of 17.5% can still be observed when extended equilibration times of 60 min are applied (Entry 9, Table 8, right). A further narrowing of the window to 20 °C to 40 °C with simultaneous extension of the holding times to 120 min still results in an actuation of 15.5% (Entry 11, Table 8, right). This extension of the equilibration times is in no way in contradiction to the intended application in a CABE. On the contrary, the temperature changes inside a wall of a building are even slower than those of the outside temperature.

To complete the thermomechanical investigations, a multi-cycle experiment (N = 30) was carried out to assess the creep behavior of the foam. For this purpose, the actuation was determined in 30 consecutive temperature cycles in the application-related temperature window between T_{low} = 15 °C and T_{high} = 40 °C. The foam again initially exhibits a pronounced thermoreversible actuation of 21.0% (N = 2). As the number of cycles increases, however. ε_{rev} decreases continuously, albeit only slightly, and still reaches a value of 19.0% in the 30th cycle (Figure 8. Supplementary Materials: Figure S11). The reason for this is probably to be found, on the one hand, in the relatively high compression rate and the associated sticking effects within the foam. On the other hand, the stronger drop in strain at the upper temperature ε_{Thigh} compared to the one at the lower temperature ε_{Tlow} indicates that at the selected T_{high} of 40 °C, a minimal percentage of the crystalline SS domains probably does not melt, and therefore, the shape recovery is not in total 100%.

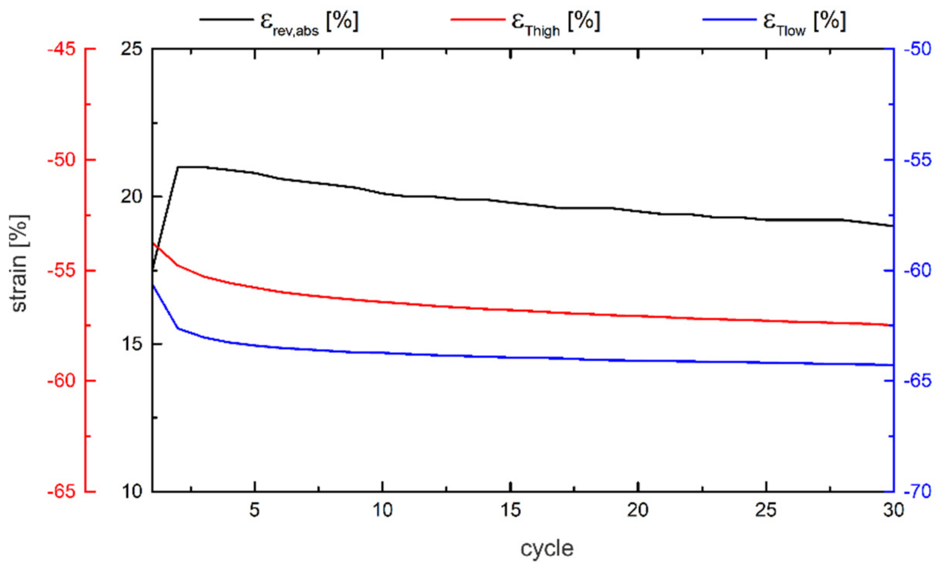

Figure 8. Investigation of the stability of 2 W actuation for PU foam in a multiple cycling experiment under constant load of 4.8 kPa (T_{high} = 40 °C and T_{low} = 15 °C).

The final step in verifying the foam functionality and demonstrating its transferability to a concept relevant to the envisioned application is performed with the aid of a demonstrator test. This is performed in analogy to our recent work [45]; we use the same demonstrator to investigate the thermoreversible actuation of the foam. For this purpose, rectangular specimens with an opening in the inside are produced by laser cutting and subjected to thermomechanical treatment in a purpose-made device. The constant stress is generated gravimetrically by applying a compressive force on the upper side of the foam with a weight of 200 g via a stamp. The compressive force is selected in such a way that the aperture closes when the lower temperature T_{low} is reached.

During the subsequent temperature cycling, a rising temperature causes an opening of the aperture, while a lowering of the temperature results in a closing (Figure 9). With a foam with the dimensions 10 × 50 × 45 mm^3, a thermoreversible actuation of 24.9% is achieved under a constant stress of 3.9 kPa. This even exceeds the actuation verified in the screening tests (Table 8), which may be traced back to a positive effect of the demonstrator design.

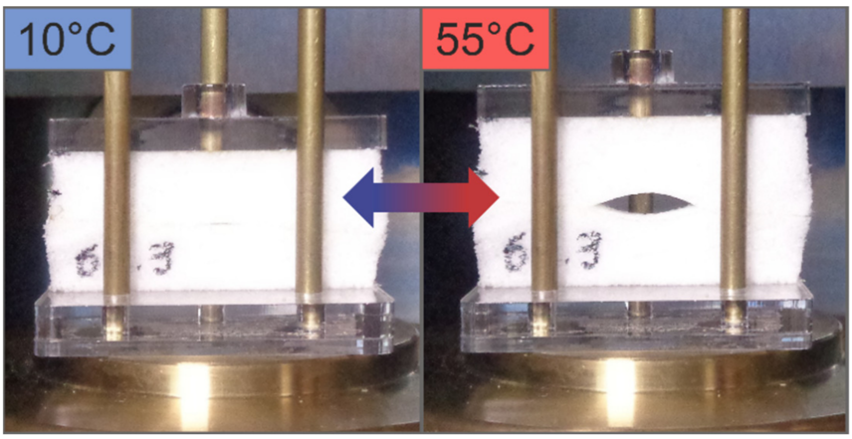

Figure 9. Thermoreversible actuation of a polyurethane foam.

The underlying principle of the exceptional magnitude of the 2W-SME observed here has not yet been fully elucidated. It is clear that the soft segmental phase transitions, including directional crystallization and melting, as well as entropy elasticity, play a decisive role [32]. However, these alone may not provide a satisfactory detailed explanation. Comparing the thermal properties, the soft segment in the PHA-based foam has a rather low enthalpy of fusion ΔH_m, with 29.0 $J \cdot g^{-1}$, compared to the already known PDA/PBA-based foam with 49.8 $J \cdot g^{-1}$ [45]. Presumably, the mixed cell structure and the interplay between open and closed cells also play a role here. The open cells allow sufficiently strong deformation to ensure the necessary rearrangement effects within the polymer chains. On the contrary, the temperature-induced pressure changes in the closed pores provide a force component supporting the cooling-induced compression and the heating-induced expansion of the foam.

As a summary of the material-specific investigations, it can be stated that it was possible to use commercially available raw materials to produce a foam with a very pronounced functionality. With a so far unprecedented thermoreversible actuation of more than 20%, a convincing thermal conductivity and a promising actuation temperature range for implementation as a functional element in a climate-adaptive building envelope (CABE) application, a promising starting point seems to have been reached for further developments and investigations.

3.3. Life Cycle Assesment

As a third perspective, the environmental sustainability of the above-presented CABE concept will be investigated in order to enable a holistic evaluation of the approach to be conducted accordingly. The life cycle assessment of the polyurethane-based shape memory polymer foam shows that the environmental impact is similar to conventional polyurethane-based polymers. In general, optimizations in the building context, e.g., in the selection of the used materials, should always be evaluated in the context of a suitable functional unit or use case. This can be a specific U-value or another building–physical variable. By referring to a defined function, the material-specific properties are considered. For example, insulation material A has a higher volume-related global warming potential (GWP) than insulation material B. However, since less material is required to fulfill a certain function, this results in a reduced impact in the context of a comparable construction.

In this case, the use of the adaptive foam element would add an additional function but also additional material to the construction. Therefore, it can only be assessed with a holistic approach, considering the effect on both the use phase as well as application in a construction.

Figure 10 shows the impact on climate change of the reference constructions' individual layers in kg CO_2-equiv. per square meter wall surface. The diagram illustrates that the addition of small volumes of SMP foam to control the flow of the air layer gap has little to no impact on the construction overall. Even in ecologically optimized constructions, the effect of the additional SMP is negligible.

As mentioned before, potential benefits are expected in the use phase because the SMP foam may influence the energy demand of a building. To assess the use phase, the energy demands for heating and cooling, calculated in the thermal simulation (Section 3.1.—Table 6), are covered by an electric heat pump (SCOP 4.9. SEER 4.7; see Section 2.3). Regardless of the fact that there are reasons for disregarding it, the additional heating energy demand for the adaptive façade concept (Table 6) is included in the calculations in its entirety. Due to the expansion of renewable energies and the resulting reduced environmental impact, a dynamic environmental profile for electricity is used for the assessment. The results are shown in Figure 11. The diagram presents the global warming potential (GWP) in kg CO_2-equiv. per square meter floor space and year. For three different locations (Holzkirchen (DE); Freiburg (DE); Madrid (ES)), the GWP is plotted over the life cycle of a ventilated ETICS compared to an unventilated ETICS. Both the effects of the production phase and the end of life remain constant over all variants.

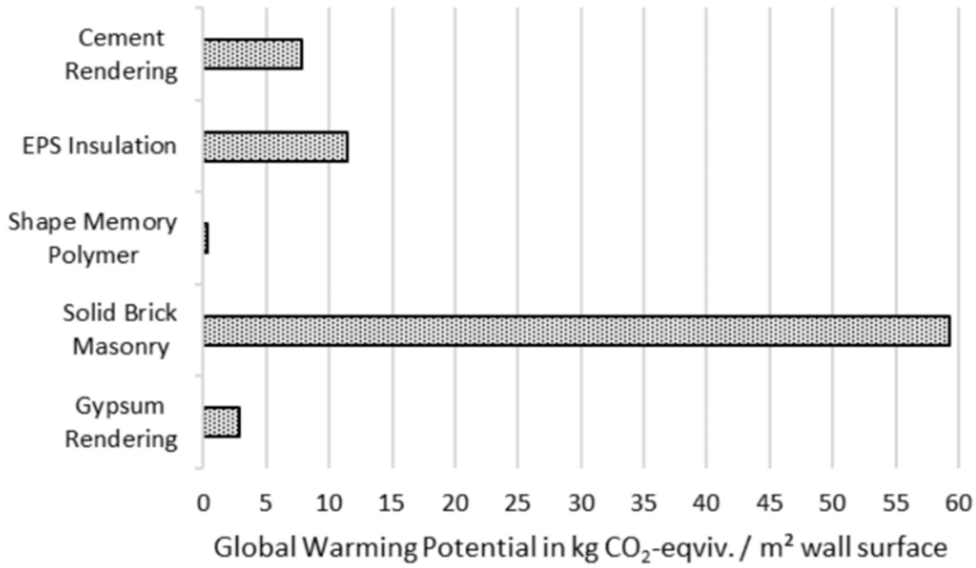

Figure 10. Impact on climate change of the individual components of the façade construction.

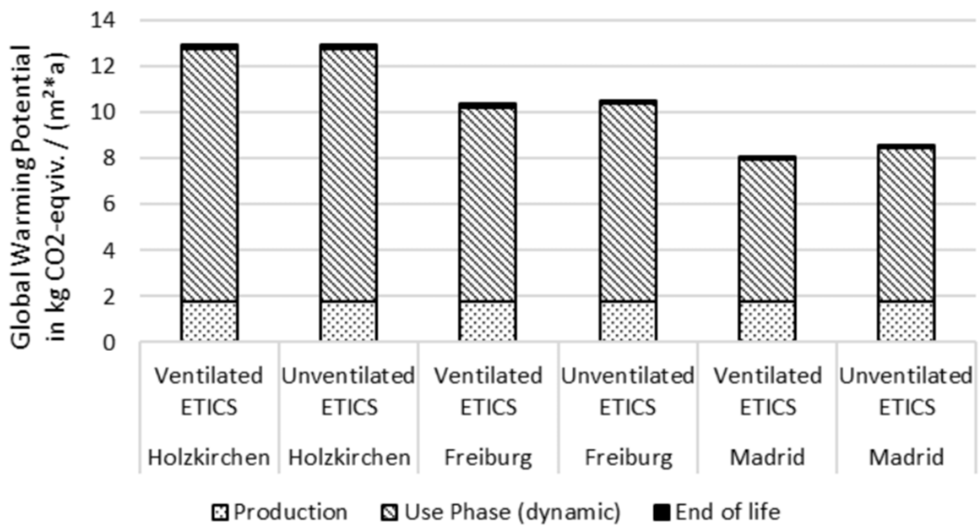

Figure 11. Impact on climate change over the life cycle of a ventilated ETICS compared to an unventilated ETICS.

The comparison of the calculated values shows, as the first aspect, that the energy demand, and therefore, the impact on climate change, varies between the different locations due to the different climatic conditions. It is also visible that the difference between the ventilated and unventilated ETICS increases the warmer the location is. For this calculation, the same SCOP and SEER is assumed for all three locations. In warmer regions, the SCOP tends to be higher, whereas the SEER tends to be lower. This would amplify the results even more.

To assess the reduction in impact on climate change and highlight meaningful use cases. Figure 12 illustrates the difference in climate change between the ventilated ETICS and the unventilated ETICS over different SCOP and SEER ratings for the three different locations. Negative percentages represent a reduced impact on climate change of the ventilated ETICS over the unventilated ETICS. For a better representation of the values, a color scale (red = worst relative value, green = best relative value) is applied to each table.

Location Holzkirchen

SEER \ SCOP	3.5	4.0	4.5	5.0	5.5	6.0
3.5	0.02%	-0.15%	-0.32%	-0.49%	-0.66%	-0.82%
4.0	0.18%	0.02%	-0.13%	-0.28%	-0.43%	-0.57%
4.5	0.29%	0.16%	0.02%	-0.11%	-0.24%	-0.38%
5.0	0.39%	0.27%	0.15%	0.02%	-0.10%	-0.22%
5.5	0.47%	0.36%	0.25%	0.13%	0.02%	-0.09%
6.0	0.53%	0.43%	0.33%	0.23%	0.13%	0.02%

Location Freiburg

SEER \ SCOP	3.5	4.0	4.5	5.0	5.5	6.0
3.5	-1.65%	-2.10%	-2.54%	-2.97%	-3.40%	-3.81%
4.0	-1.24%	-1.65%	-2.04%	-2.43%	-2.81%	-3.19%
4.5	-0.92%	-1.29%	-1.65%	-2.00%	-2.35%	-2.69%
5.0	-0.66%	-0.99%	-1.32%	-1.65%	-1.96%	-2.28%
5.5	-0.44%	-0.75%	-1.05%	-1.35%	-1.65%	-1.94%
6.0	-0.26%	-0.55%	-0.83%	-1.10%	-1.38%	-1.65%

Location Madrid

SEER \ SCOP	3.5	4.0	4.5	5.0	5.5	6.0
3.5	-7.05%	-7.97%	-8.81%	-9.58%	-10.29%	-10.96%
4.0	-6.18%	-7.05%	-7.86%	-8.60%	-9.30%	-9.94%
4.5	-5.46%	-6.28%	-7.05%	-7.77%	-8.44%	-9.07%
5.0	-4.85%	-5.63%	-6.36%	-7.05%	-7.70%	-8.31%
5.5	-4.32%	-5.06%	-5.77%	-6.43%	-7.05%	-7.64%
6.0	-3.86%	-4.57%	-5.24%	-5.88%	-6.48%	-7.05%

Figure 12. Difference in climate change between ventilated and unventilated ETICS.

First of all, it is noticeable that the ventilated ETICS does not always perform better than the unventilated ETICS. In general, the benefit increases with higher SCOP and decreases with higher SEER. This is because the use of the ventilated ETICS causes higher heating demand but decreases the demand for cooling. This effect is amplified in warmer regions.

Especially in the rather cool climate of Holzkirchen, multiple coefficient combinations emerge under which the CABE concept performs worse than the static concept. The values for the change in impact span from +0.53% to −0.82%. For the warmer climate in Freiburg, a positive effect is obtained across all combinations considered, which can be quantified with values from −0.26% to −3.81%. As expected, the greatest benefit is attained under the warmest climatic conditions. For Madrid, improvements in the range of −3.86% to −10.96% are achieved, and thus, significant reductions in the ecological impact.

4. Discussion

The simulations show that a ventilated ETICS can improve the thermal comfort in non-air-conditioned residential buildings. The degree of this improvement depends to a large extent on the climatic conditions. At the same time, the cooling energy saving potentials of 29% to 45%, depending on the location, identified under the model assumptions made, clearly indicate that such an innovative concept can contribute valuably to the achievement of global climate goals.

In order to improve the accuracy of the predictions, further investigations and an optimization of the simulation processes are necessary. For example, an adaptable switching criterion and a targeted adaptation of the boundary conditions to the climate scenario under investigation may further increase the validity and possibly have a beneficial effect on the results. A more precise and case-specific evaluation of the optimal switching conditions would then allow the formulation of precise fitting material requirements. Ultimately, however, field tests under real-life conditions must be carried out. They provide the best way to obtain more precise and practical information on the behavior of a ventilated ETICS. Here, the temperature profiles, the wind influence, as well as the flow resistance, could be analyzed in detail.

With the investigated PU-based SMP foam and its remarkable thermoreversible actuation capability of more than 20%, a substantiated material basis was established, which even allows a fine-tuning of physical properties. By varying the SS building block and making adjustments to the formulation, the switching temperature range can be tailored for specific applications. If a deeper insight into the structure–function relationships can be gained, this also offers the possibility of further optimizing the SMP material, e.g., its pore structure and the design of novel programmable materials. Based on this, further application scenarios can be addressed, which, in addition to thermal management, also include application areas, such as actuators and morphing structures.

From an environmental perspective, there appears to be a great potential in adaptive foam elements in building applications to reduce the impact on climate change. The big advantage in the use phase is countered by a merely small to negligible disadvantage in the footprint of the construction itself. Undoubtedly, the location and the efficiencies of the heating and cooling systems must always be taken into account. Nevertheless, the LCAs carried out imply that the CABE concept presented here has a beneficial effect on the sustainability of building envelopes, especially in rather warm climatic regions, and thus represents another persuasive argument that can initiate a trend toward programmable materials in the building sector.

5. Conclusions

The CABE concept presented here embodies a novel approach to implementing material-inherent thermal management in a thermal insulation composite system. The thermoreversible shape change of a SMP foam enables an autonomous adaptation to the prevailing environmental conditions. The attainable benefit of such a concept in the context of a building envelope, as demonstrated by the various simulation results, underlines the potential of programmable materials to contribute to increased energy efficiency. The unique ability of programmable materials to reversibly change their properties and behaviors according to a program in an autonomous and predetermined way is not only the key to novel solutions and approaches in various contexts. It can also pave the way for a future paradigm shift in materials science. In the end, the programming of a material enables the programming of a functionality.

Supplementary Materials: The following supporting information can be downloaded at: https://www.mdpi.com/article/10.3390/buildings12122236/s1. Figure S1: Principal drawing of the investigated apartment in a multi-story apartment building; Figure S2: ACH rates inside the ventilation space behind the ventilated ETICS for Holzkirchen (DE); Figure S3: ACH rates inside the ventilation space behind the ventilated ETICS for Freiburg (DE); Figure S4: ACH rates inside the ventilation space behind the ventilated ETICS for Madrid (ES); Figure S5: Air temperatures inside the air layer gap with a ventilated ETICS (blue) and an unventilated ETICS (red) for Holzkirchen (DE); Figure S6: Air temperatures inside the air layer gap with a ventilated ETICS (blue) and an unventilated ETICS (red) for Freiburg (DE); Figure S7: Air temperatures inside the air layer with a ventilated ETICS (blue) and an unventilated ETICS (red) for Madrid (ES); Figure S8: DSC thermograms of pure PHA (black) and the corresponding PU foam (red); Figure S9: Influence of compressive stress and temperature holding conditions on thermoreversible actuation of the PU foam; Figure S10: Overview of the investigations on the temperature dependency of the 2W-SME—(a) variation of T_{high} and (b) variation of T_{low}; Figure S11: Multiple cycling experiments.

Author Contributions: Conceptualization. S.L.-B., K.L., D.B., S.A. and M.W.; methodology. K.L., D.B. and M.W.; software. K.L., P.K. and D.B.; validation. K.L., P.K., D.B., S.A. and M.W.; formal analysis. K.L., D.B. and M.W.; investigation. K.L., D.B. and M.W.; writing—original draft preparation. K.L., P.K., D.B., S.A. and M.W.; writing—review and editing. M.K., T.P. and M.W.; visualization. K.L., D.B. and M.W.; supervision. M.W.; project administration. S.L.-B., T.P. and M.W.; funding acquisition. S.L.-B. and T.P. All authors have read and agreed to the published version of the manuscript.

Funding: This research was funded by the Fraunhofer Cluster of Excellence "Programmable Materials". grant number 630519 (PSP element 40-03549-2500-00002).

Data Availability Statement: Not applicable.

Acknowledgments: T.P. wishes to thank the European Regional Development Fund for financing parts of the laboratory equipment (project 85007031). Tobias Rümmler is kindly acknowledged for carrying out the DMA measurements and demonstrator trials.

Conflicts of Interest: The authors declare no conflict of interest. The funders had no role in the design of the study; in the collection. analyses. or interpretation of data; in the writing of the manuscript. or in the decision to publish the results.

Appendix A

Appendix A.1. Detailed Information on Materials and Foam Preparation

The polyester Diexter G 240 is kindly provided by C.O.I.M. (Offanengo. Italy). It is a linear polyol. which consists of poly(1.6-hexylene adipate) (PHA) with a molecular weight of 2970 g/mol. Dibutyltin dilaurate (DBTL) and 4.4′-diphenylmethane diisocyanate (MDI) are purchased from Fisher Scientific (Schwerte. Germany) and diethanolamine (DEA) from Merck Millipore (Darmstadt. Germany). The surfactant Tegostab B8407 is obtained from Evonik (Essen. Germany) and the antioxidant Irganox 1076 from BASF (Ludwigshafen. Deutschland). MDI is melted and decanted before use in order to remove solid residues and contaminants. The other materials are used as received. Deionized water is used as the chemical blowing agent.

The polymer foam is synthesized via a one-pot two-step reaction from PHA diol in the presence of a slight excess of MDI with a ratio of NCO/OH = 1.03. Therefore. PHA is dried under vacuum overnight at 85 °C in a 650 mL polypropylene beaker. The polymer melt is placed on a heating plate and stirred for 2 min at 80 °C using a mechanical stirrer. After adding the surfactant (2.0 pphp). antioxidant (0.2 pphp) and gelling catalyst (0.5 pphp). molten MDI (31.3 pphp) is added under vigorous stirring. After 30 s. a mixture of DEA (1.25 pphp) and deionized water (1.25 pphp) is added at high stirring speed to finalize the reaction and initiate the foaming process. Once significant foaming occurs. the stirrer is removed to enable the free rise of the foam. The freshly prepared foam is kept overnight at 23 °C for post-curing.

Different sized samples are taken from the center of the foam using a band saw (HBS230HQ. Holzmann Maschinen GmbH. Haslach. Austria).

Appendix A.2. Detailed Description of Characterization Methods

The thermal properties of polyester diols and polyurethane (PU) foam are investigated by DSC using a Q100 DSC (TA Instruments. New Castle. DE. USA). The polyol samples weigh approximately 5 mg. while the foam samples have a weight of roughly 3 mg. Two thermal cycles with heating and cooling rates of 10 K·min^{-1} are performed for each DSC measurement. The temperature area ranges from −20 °C to 100 °C for the polyester diol and from −70 °C to 100 °C for the PU foam. The first cycle is performed to eliminate the thermal history. while the measured data from the second cooling and heating are used to study the phase transitions. In addition. the crystallization behavior of the foam under isothermal condition is investigated at different temperatures. For this purpose. the sample is cooled in each case from 65 °C at a maximum cooling rate of 100 K·min^{-1} to the respective storage temperature T_{store} where it is stored for 30 min.

A DMA experiment is run in strain mode in order to determine the mechanical behavior. hardness and compressive strength of the foam. In the first and second cycle. the specimen is deformed at 20 °C with a compression rate of 10%·min^{-1} until a maximum deformation of 60% is achieved. After 5 min under these conditions. unloading is accomplished at a rate of 5%·min^{-1}. Before the third cycle. the specimen is heated to 45 °C at 5 K·min^{-1} and equilibrated for 15 min. This is followed by another 60% compression. including equilibration and subsequent unloading.

The shape memory properties are characterized by means of DMA measurements in controlled force mode. The programming of the samples is accomplished by thermomechanical treatment. For this purpose. the sample is heated from 23 °C to the deformation temperature T_d = 60 °C. where it is kept for 30 min and then exposed to a specific load with a rate of 2 N·min^{-1}. The temperature is then maintained for 15 min. after which the initial height h_{high} of the foam at T_{high} is recorded. Subsequently. actuation in relation to changes in h_{high} is investigated under constant load conditions. Therefore. the same is cooled to T_{low} = 0 °C. where it is kept for 30 min. and the height h_{low} of the foam at T_{low} is recorded before it is reheated to T_{high} = 60 °C. followed by one further temperature conditioning of 30 min.

For the force screening. loads of 0.5 N. 1.0 N. 1.5 N. 2.0 N. 5.0 N and 10.0 N are imposed. In each case. the thermal cycling is repeated twice between T_{low} and T_{high}. corresponding to a cycle number of N = 3.

The temperature screening is performed with a constant load of 0.5 N. The temperature ranges as well as the equilibration times are varied. Values of 35 °C. 40 °C. 45 °C. 50 °C and 55 °C are investigated for the upper temperature T_{high} and values of 0 °C. 5 °C. 10 °C. 15 °C and 20 °C for the lower temperature T_{low}. The equilibration times are extended up to 120 min with decreasing T_{high} and increasing T_{low}. respectively. Thermal cycles are each repeated once (N = 2). Heating and cooling rates are set to 5 K·min^{-1}. while a loading rate of 2 N·min^{-1} is applied.

The multiple cycling experiment is carried out analogously to the temperature screening and with a load of 0.5 N. A series of 30 consecutive thermal cycles between T_{low} = 15 °C and T_{high} = 40 °C are performed (N = 30) with holding times of 60 min.

References

1. GlobalABC. GlobalABC Roadmap for Buildings and Construction 2020–2050. Paris. 2020. Available online: https://www.iea.org/reports/globalabc-roadmap-for-buildings-and-construction-2020-2050 (accessed on 4 October 2022).
2. IEA. Cooling. Paris. 2021. Available online: https://www.iea.org/reports/cooling (accessed on 4 October 2022).
3. IEA. The Future of Cooling. Paris. 2018. Available online: https://www.iea.org/reports/the-future-of-cooling (accessed on 4 October 2022).
4. Loonen, R.C.G.M.; Trčka, M.; Cóstola, D.; Hensen, J.L.M. Climate adaptive building shells: State-of-the-art and future challenges. *Renew. Sustain. Energy Rev.* **2013**, *25*, 483–493. [CrossRef]
5. Sadineni, S.B.; Madala, S.; Boehm, R.F. Passive building energy savings: A review of building envelope components. *Renew. Sustain. Energy Rev.* **2011**, *15*, 3617–3631. [CrossRef]
6. Perino, M.; Serra, V. Switching from static to adaptable and dynamic building envelopes: A paradigm shift for the energy efficiency in buildings. *J. Facade Des. Eng.* **2015**, *3*, 143–163. [CrossRef]
7. Luo, Y.; Zhang, L.; Bozlar, M.; Liu, Z.; Guo, H.; Meggers, F. Active building envelope systems toward renewable and sustainable energy. *Renew. Sustain. Energy Rev.* **2019**, *104*, 470–491. [CrossRef]
8. Zamovskis, M.; Vanaga, R.; Blumberga, A. Mathematical Modelling of Performance of New Type of Climate Adaptive Building Shell. *Energy Procedia* **2017**, *113*, 270–276. [CrossRef]
9. Taveres-Cachat, E.; Grynning, S.; Thomsen, J.; Selkowitz, S. Responsive building envelope concepts in zero emission neighborhoods and smart cities—A roadmap to implementation. *Build. Environ.* **2019**, *149*, 446–457. [CrossRef]
10. Hu, J.; Yu, X. Thermo and light-responsive building envelope: Energy analysis under different climate conditions. *Sol. Energy* **2019**, *193*, 866–877. [CrossRef]
11. Kim, H.; Clayton, M.J. Parametric behavior maps: A method for evaluating the energy performance of climate-adaptive building envelopes. *Energy Build.* **2020**, *219*, 110020. [CrossRef]
12. Berge, A.; Hagentoft, C.-E.; Wahlgren, P.; Adl-Zarrabi, B. Effect from a Variable U-Value in Adaptive Building Components with Controlled Internal Air Pressure. *Energy Procedia* **2015**, *78*, 376–381. [CrossRef]

13. Favoino, F.; Jin, Q.; Overend, M. Design and control optimisation of adaptive insulation systems for office buildings. Part 1: Adaptive technologies and simulation framework. *Energy* **2017**, *127*, 301–309. [CrossRef]
14. Mazar, M.M.; Rezaeizadeh, A. Adaptive model predictive climate control of multi-unit buildings using weather forecast data. *J. Build. Eng.* **2020**, *32*, 101449. [CrossRef]
15. Alkhatib, H.; Lemarchand, P.; Norton, B.; O'Sullivan, D.T.J. Deployment and control of adaptive building facades for energy generation. thermal insulation. ventilation and daylighting: A review. *Appl. Therm. Eng.* **2021**, *185*, 116331. [CrossRef]
16. Sobek, W.; Sawodny, O.; Bischoff, M.; Blandini, L.; Böhm, M.; Haase, W.; Klett, Y.; Mahall, M.; Weidner, S.; Burghardt, T.; et al. Adaptive Hüllen und Strukturen. *Bautechnik* **2021**, *98*, 208–221. [CrossRef]
17. Harder, N.; Schlegl, F.; Flemming, D.; di Bari, R.; Albrecht, S.; Leistner, P.; Park, S. Bauphysikalische und ökologische Bewertung adaptiver Fassadenkonstruktionen auf Raumebene. *Bauphysik* **2019**, *41*, 302–313. [CrossRef]
18. Harder, N.; Schlegl, F.; Albrecht, S.; Park, S.; Leistner, P. Bauphysikalische und ökologische Potenziale von adaptiven Leichtbaukonstruktionen. *Bauphysik* **2018**, *40*, 307–318. [CrossRef]
19. Smith, S.I. Superporous Intelligent Hydrogels for Environmentally Adaptive Building Skins. *MRS Adv.* **2017**, *2*, 2481–2488. [CrossRef]
20. Di Maggio, R.; Dirè, S.; Callone, E.; Bergamonti, L.; Lottici, P.P.; Albatici, R.; Rigon, R.; Ataollahi, N. Super-adsorbent polyacrylate under swelling in water for passive solar control of building envelope. *SN Appl. Sci.* **2020**, *2*, 1–13. [CrossRef]
21. Zhou, Y.; Wang, S.; Peng, J.; Tan, Y.; Li, C.; Boey, F.Y.C.; Long, Y. Liquid Thermo-Responsive Smart Window Derived from Hydrogel. *Joule* **2020**, *4*, 2458–2474. [CrossRef]
22. Al Athas, S.I. Optimization Study of Parametric Thermal Bimetal Material Module for Green Building in Tropical Humid Climate. *Acad. Res. Community Publ.* **2019**, *3*, 240. [CrossRef]
23. Li, Z.; Zhang, S.; Chang, J.; Zhao, F.; Zhao, Y.; Gao, J. Simulation study on light environment performance and heat gain of applying a bimetal automatic shading device to rooms. *Energy Build.* **2020**, *211*, 109820. [CrossRef]
24. Granqvist, C.G. Electrochromics and Thermochromics: Towards a New Paradigm for Energy Efficient Buildings. *Mater. Today Proc.* **2016**, *3*, S2–S11. [CrossRef]
25. Akeiber, H.; Nejat, P.; Majid, M.Z.A.; Wahid, M.A.; Jomehzadeh, F.; Zeynali Famileh, I.; Calautit, J.K.; Hughes, B.R.; Zaki, S.A. A review on phase change material (PCM) for sustainable passive cooling in building envelopes. *Renew. Sustain. Energy Rev.* **2016**, *60*, 1470–1497. [CrossRef]
26. Hu, J.; Yu, X. Adaptive building roof by coupling thermochromic material and phase change material: Energy performance under different climate conditions. *Constr. Build. Mater.* **2020**, *262*, 120481. [CrossRef]
27. Lengsfeld, K.; Walter, M.; Krus, M.; Pappert, S.; Teicht, C. Innovative Development of Programmable Phase Change Materials and Their Exemplary Application. *Energies* **2021**, *14*, 3440. [CrossRef]
28. Chang, W.-S.; Araki, Y. Use of shape-memory alloys in construction: A critical review. *Proc. Inst. Civ. Eng. Civ. Eng.* **2016**, *169*, 87–95. [CrossRef]
29. Yi, H.; Kim, D.; Kim, Y.; Kim, D.; Koh, J.-s.; Kim, M.-J. 3D-printed attachable kinetic shading device with alternate actuation: Use of shape-memory alloy (SMA) for climate-adaptive responsive architecture. *Autom. Constr.* **2020**, *114*, 103151. [CrossRef]
30. Clifford, D.T.; Zupan, R.J.; Brigahm, J.C.; Bebbow, R.V.; Whittock, M.; Davis, N. Application of shape-memory polymers to climate adaptive building facades. In Proceedings of the 12th Conference of Advanced Building Skins, Bern, Switzerland, 2–3 October 2017.
31. Li, J.; Duan, Q.; Zhang, E.; Wang, J. Applications of Shape Memory Polymers in Kinetic Buildings. *Adv. Mater. Sci. Eng.* **2018**, *2018*, 1–13. [CrossRef]
32. Chung, T.; Romo-Uribe, A.; Mather, P.T. Two-Way Reversible Shape Memory in a Semicrystalline Network. *Macromolecules* **2008**, *41*, 184–192. [CrossRef]
33. Bothe, M.; Pretsch, T. Two-Way Shape Changes of a Shape-Memory Poly(ester urethane). *Macromol. Chem. Phys.* **2012**, *213*, 2378–2385. [CrossRef]
34. Bothe, M.; Pretsch, T. Bidirectional actuation of a thermoplastic polyurethane elastomer. *J. Mater. Chem. A* **2013**, *1*, 14491. [CrossRef]
35. Behl, M.; Kratz, K.; Zotzmann, J.; Nöchel, U.; Lendlein, A. Reversible bidirectional shape-memory polymers. *Adv. Mater.* **2013**, *25*, 4466–4469. [CrossRef]
36. Lendlein, A.; Gould, O.E.C. Reprogrammable recovery and actuation behaviour of shape-memory polymers. *Nat. Rev. Mater.* **2019**, *4*, 116–133. [CrossRef]
37. Zare, M.; Prabhakaran, M.P.; Parvin, N.; Ramakrishna, S. Thermally-induced two-way shape memory polymers: Mechanisms. structures. and applications. *Chem. Eng. J.* **2019**, *374*, 706–720. [CrossRef]
38. Schönfeld, D.; Chalissery, D.; Wenz, F.; Specht, M.; Eberl, C.; Pretsch, T. Actuating Shape Memory Polymer for Thermoresponsive Soft Robotic Gripper and Programmable Materials. *Molecules* **2021**, *26*, 522. [CrossRef] [PubMed]
39. Fiorito, F.; Sauchelli, M.; Arroyo, D.; Pesenti, M.; Imperadori, M.; Masera, G.; Ranzi, G. Shape morphing solar shadings: A review. *Renew. Sustain. Energy Rev.* **2016**, *55*, 863–884. [CrossRef]
40. Yoon, J. Design-to-fabrication with thermo-responsive shape memory polymer applications for building skins. *Archit. Sci. Rev.* **2021**, *64*, 72–86. [CrossRef]

41. Barozzi, M.; Lienhard, J.; Zanelli, A.; Monticelli, C. The Sustainability of Adaptive Envelopes: Developments of Kinetic Architecture. *Procedia Eng.* **2016**, *155*, 275–284. [CrossRef]
42. Lee, D.-S.; Koo, S.-H.; Seong, Y.-B.; Jo, J.-H. Evaluating Thermal and Lighting Energy Performance of Shading Devices on Kinetic Façades. *Sustainability* **2016**, *8*, 883. [CrossRef]
43. Premier, A. Solar shading devices integrating smart materials: An overview of projects. prototypes and products for advanced façade design. *Archit. Sci. Rev.* **2019**, *62*, 455–465. [CrossRef]
44. Shahin, H.S.M. Adaptive building envelopes of multistory buildings as an example of high performance building skins. *Alex. Eng. J.* **2019**, *58*, 345–352. [CrossRef]
45. Walter, M.; Friess, F.; Krus, M.; Zolanvari, S.M.H.; Grün, G.; Kröber, H.; Pretsch, T. Shape Memory Polymer Foam with Programmable Apertures. *Polymers* **2020**, *12*, 1914. [CrossRef] [PubMed]
46. Holm, A.; Radon, J.; Künzel, H.; Sedlbauer, K. *Berechnung des Hygrothermischen Verhaltens von Räumen*; WTA-Publication No. 24: München, Germany, 2004.
47. Lengsfeld, K.; Holm, A. Entwicklung und Validierung einer hygrothermischen Raumklima-Simulationssoftware WUFI®-Plus. *Bauphysik* **2007**, *29*, 178–186. [CrossRef]
48. WUFI®implemented hygrothermal reference year (HRY).
49. *DIN EN 12664:2001-05*; Wärmetechnisches Verhalten von Baustoffen und Bauprodukten: Bestimmung des Wärmedurchlasswiderstandes nach dem Verfahren mit dem Plattengerät und dem Wärmestrommessplatten-Gerät Trockene und feuchte Produkte mit mittlerem und niedrigem Wärmedurchlasswiderstand. Deutsche Fassung EN_12664:2001; Beuth Verlag GmbH: Berlin, Germany, 2001.
50. *DIN EN ISO 14040:2009-11*; Umweltmanagement-Ökobilanz-Grundsätze und Rahmenbedingungen (ISO_14040:2006). Deutsche und Englische Fassung EN_ISO_14040:2006; Beuth Verlag GmbH: Berlin, Germany, 2009.
51. *DIN EN ISO 14044:2018-05*; Umweltmanagement_- Ökobilanz_- Anforderungen und Anleitungen (ISO_14044:2006_+ Amd_1:2017). Deutsche Fassung EN_ISO_14044:2006_+ A1:2018; Beuth Verlag GmbH: Berlin, Germany, 2018.
52. GaBi. Sphera Solutions. Inc. Available online: https://gabi.sphera.com/international/software/ (accessed on 15 February 2022).
53. GENERIS®. Fraunhofer Institut für Bauphysik IBP. 2022. Available online: https://www.generis-solution.eu/ (accessed on 15 February 2022).
54. DGNB Certification System. German Sustainable Building Council: Stuttgart. Available online: https://www.dgnb-system.de/en/ (accessed on 15 February 2022).
55. Building Research Establishment Environmental Assessment Method (BREEAM). Building Research Establishment (BRE): UK. Available online: https://bregroup.com/products/breeam/ (accessed on 15 February 2022).
56. Bundesministerium des Innern. für Bau und Heimat. ÖKOBAUDAT Datenbank. Available online: https://www.oekobaudat.de/ (accessed on 15 February 2022).
57. *DIN EN 15804:2020-03*; Nachhaltigkeit von Bauwerken-Umweltproduktdeklarationen-Grundregeln für die Produktkategorie Bauprodukte. Deutsche Fassung EN_15804:2012+A2:2019; Beuth Verlag GmbH: Berlin, Germany, 2020.
58. *DIN EN 15978:2012-10*; Nachhaltigkeit von Bauwerken-Bewertung der umweltbezogenen Qualität von Gebäuden-Berechnungsmethode. Deutsche Fassung EN_15978:2011; Beuth Verlag GmbH: Berlin, Germany, 2012.
59. Shirole, A.; Perotto, C.U.; Balog, S.; Weder, C. Tailoring the Shape Memory Properties of Segmented Poly(ester urethanes) via Blending. *ACS Appl. Mater. Interfaces* **2018**, *10*, 24829–24839. [CrossRef] [PubMed]
60. Karasu, F.; Weder, C. Tuning the Properties of Shape-Memory Polyurethanes via the Nature of the Polyester Switching. *Segment. Macromol. Mater. Eng.* **2021**, *306*, 2000770. [CrossRef]
61. Federation of European Rigid Polyurethane Foam Associations. *Thermal Insulation Materials Made of Rigid Polyurethane Foam (PUR/PIR)—Properties—Manufacture (Report N°1. October 06)*; Federation of European Rigid Polyurethane Foam Associations: Brussels, Belgium, 2006.
62. Li, G.; Wang, A. Cold, warm, and hot programming of shape memory polymers. *J. Polym. Sci. Part B Polym. Phys.* **2016**, *54*, 1319–1339. [CrossRef]